

VARIABLE-RANGE HOPPING CONDUCTION IN THE $\text{Cu}_2\text{Zn}_{1-x}\text{Cd}_x\text{SnS}_4$ SINGLE CRYSTALS

V. BATIR^{1,*}, K. G. LISUNOV^{1,2}, E. ARUSHANOV¹

¹ Institute of Applied Physics, Moldova State University, 5 Academiei str., MD 2028, Chisinau, Republic of Moldova

² Lappeenranta University of Technology, PO Box 20, FIN-53851 Lappeenranta, Finland

* Author to whom correspondence should be addressed: batir.valentin@usm.md

Received September 24, 2025

Abstract. Resistivity, $\rho(T)$, of the $\text{Cu}_2\text{Zn}_{1-x}\text{Cd}_x\text{SnS}_4$ (CZCTS) solid solutions is investigated within the temperature range of 10-300 K. The nearest-neighbor hopping (NNH) conductivity is observed within the temperature interval of ~110-190 K, whereas the Mott variable-range hopping (VRH) conductivity is identified in the temperature range of ~60 -140 K. Analysis of the resistivity separately in the NNH and the Mott VRH conduction regimes have yielded the values of the NNH activation energy, $E_n \approx 22\text{-}68$ meV, the semi-width of the acceptor band, $W \approx 9\text{-}58$ meV, the relative acceptor concentration, $N/N_c \approx 0.27\text{-}0.80$, where N_c is the critical concentration of the metal-insulator transition (MIT), and the localization radius in units of that far from the MIT, $a/a_0 \approx 1.4\text{-}4.9$.

Key words: $\text{Cu}_2\text{ZnSnS}_4$, $\text{Cu}_2\text{CdSnS}_4$, kesterites, single crystals, conductivity mechanisms.

1. INTRODUCTION

During the last time, researchers have focused on searching for and investigating new compounds with useful properties. The goal is to replace less effective, expensive, and environmentally unsustainable materials in various important applications, particularly in the fabrication of solar cells [1]. In this context, kesterites have attracted considerable interest in the last two decades due to the earth abundances of their elements in the crust, low cost, and high flexibility of physicochemical properties [2,3]. Therefore, $\text{Cu}_2\text{ZnSnS}_4$ (CZTS), one of the most investigated members of the kesterite family of compounds, exhibits an optimum band gap of ~1.5 eV and a high absorption coefficient of $\sim 10^4$ cm⁻¹ [4,5], containing

mainly abundant elements with low toxicity. The maximum power conversion efficiency obtained for this compound, has reached 13.2% for a lithium-doped device [6].

However, the potential of this semiconductor is somewhat limited by the adverse effects of Cu_{Zn} antisite defects [7]. These defects are primarily responsible for reducing the minority carrier lifetime, causing variations in the electrostatic potential, and leading to the emergence of band tail states [8–10]. All of these factors play a crucial role in formation of the conversion efficiency in kesterite solar cells. Additionally, the Cu_{Zn} antisite defects were found to be responsible for the formation of a defect acceptor band (AB) inside the band gap of the material [11–14]. These lattice defects in kesterites are primarily associated with Cu–Zn disorder, which can even result in a new structural type or a disordered kesterite [15].

Researchers have explored different strategies to mitigate the negative impact of these defects. One of them suggests a partial or complete substitution of Sn with Ge and S with Se in the cation and anion subsystems, respectively. This procedure permits a band gap tuning within limits of ~ 1.0 – 2.4 eV, enhancing the conversion efficiency of $\text{Cu}_2\text{ZnSn}_x\text{Ge}_{1-x}(\text{S}_y\text{Se}_{1-y})_4$ solar cells above 12% [16–19]. However, these efforts have not been very successful in significantly reducing the concentration of Cu_{Zn} defects.

A more direct method utilizes the partial substitution of Zn with Cd [20–23]. Because of the larger ionic radius of Cd^{2+} (0.94 Å) compared with that of Zn^{2+} (0.74 Å) [24,25], it has been supposed that Cd substitution could lower the concentration of Cu_{Zn} antisite defects [7,26,27]. Moreover, this partial substitution of Zn with Cd has led to promising solar cell efficiencies above 11.5% [7,26,28].

However, the exact nature of Cd beneficial effect remains debated, as DFT calculations suggest that replacing Zn with Cd does not significantly increase the formation energy of $\text{Cu}_{\text{Zn}/\text{Cd}} + \text{Zn}/\text{Cd}_{\text{Cu}}$ defects [29].

Contrary to expectations, substituting Zn with Cd at the 2d Wyckoff sites does not take place in the $\text{Cu}_2\text{ZnSnS}_4$ structure. Instead, due to the continuous transformation of the structure from the kesterite to stannite type with increased Cd substitution, Cd replaces Cu at the 2a sites, whereas Cu moves to the Zn 2d positions [30]. Additionally, XRD analysis revealed a phase transition from the kesterite to the stannite structure, when over 60% of Zn in the CZCTS solid solutions was replaced by Cd [26].

This discrepancy between the theoretical and experimental results necessitates a more thorough examination of how Cd substitution affects the properties of CZCTS solid solutions. Consequently, there is still a lack of information regarding the impact of Cd substitution on the transport properties of these compounds.

In the present study, investigations of the resistivity, $\rho(T)$ of the $\text{Cu}_2\text{Zn}_{1-x}\text{Cd}_x\text{SnS}_4$ (CZCTS) single crystals were performed within a temperature range of 10–300 K. Detailed analysis of $\rho(T)$ allowed to identify the main conduction

mechanisms in this material and to obtain important microscopic parameters characteristic of the defect AB.

2. EXPERIMENTAL DETAILS

2.1. CRYSTAL GROWTH

Single crystals of CZCTS solid solutions were prepared in two steps using the chemical vapor transport (CVT) method. In the synthesis procedure, elemental components with high purity (99.999%) were utilized, while iodine at a concentration of 5 mg/cm^3 served as the transport medium.

In the first step, elemental components such as copper, zinc, cadmium, tin, and sulfur were weighed in stoichiometric proportions and used as starting materials to synthesize polycrystalline CZCTS compounds through solid-state reactions. Afterward, the polycrystalline ingots were ground and loaded into quartz ampoules evacuated to a residual pressure of about 10^{-3} Pa. The internal diameter of the ampoules was approximately 16-22 mm, while their length was about 170 mm.

In order to form metal iodides and eliminate potential uncontrolled crystallization centers, the ampoules were placed in a horizontal two-zone furnace, where the temperatures of the reaction and crystallization zones were equal to 670 K and 740 K, respectively. The ampoules were maintained at these temperatures for 2-3 days, after which the temperature was equalized across the ampoule and kept at 970 K for 24 h.

Finally, the temperature in the reaction zone was gradually increased to 1070 K over 170 h, and the growth process continued for 240 h.

2.2. MEASUREMENTS PERFORMING

The chemical compositions of the investigated specimens were determined from the X-ray fluorescence spectra using the "X-Calibur" Xenometrix system. The system was equipped with an X-ray source with a Rh target and an SDD detector, which offered a resolution of 135 keV. The sample composition was calculated using an integrated software.

The temperature dependence of the resistivity was measured between 10 and 300 K using a standard dc method. For this purpose, four silver-paste contacts were made, and each sample was fixed on a circular platform to avoid contact damage.

The sample temperature was varied in a closed-cycle He cryostat connected to a temperature controller Lakeshore 335. At the same time, resistivity measurements were performed, using a GDM-8261 dual measurement multimeter from GWInstek.

All measurements were done in automatic mode, which provided higher precision and collection of a sufficient amount of data for analysis.

3. RESULTS AND DISCUSSION

3.1. CHEMICAL COMPOSITION

The chemical composition of the CZCTS single crystals, measured by means of XRF spectroscopy is presented in Table 1. In this table, a slight excess of Cu ($\text{Cu}/(\text{Zn}+\text{Cd}+\text{Sn}) > 1$) can be observed for samples S1, S3 and S6, while samples S4, S7 and S8 are characterized by a slightly poor content of Cu. The only samples that show reasonable Cu content ($\text{Cu}/(\text{Zn}+\text{Cd}+\text{Sn}) \approx 1$), are S2 and S5.

Additionally, a slight excess of Zn+Cd was observed for S3 and S5, while for the rest of the samples the sum of Zn+Cd exhibits a slight deficit.

Finally, it has been found that there are some deviations between the nominal value of x and the observed ratio of Cd/(Zn+Cd) in the investigated samples. In particular, the most significant deviations were observed for S2, S3, S4 and S5 samples, ranging from 0.08 to 0.12.

In contrast, the rest of the samples showed a good agreement between the Cd/(Zn+Cd) ratio and initial loading.

Table 1.

Chemical composition of the investigated CZCTS samples measured by XRF.

Sample	Cu (at. %)	Zn (at. %)	Cd (at. %)	Sn (at. %)	S (at. %)	Cd/ (Zn+Cd)	Cu/ (Zn+Cd+Sn)	(Zn+Cd) /Sn
S1	18.42	8.61	0.00	9.09	63.87	0.00	1.04	0.95
S2	18.40	7.24	1.68	9.45	63.23	0.19	1.00	0.94
S3	18.34	6.23	2.93	9.04	63.47	0.32	1.01	1.01
S4	22.40	8.57	5.34	15.80	47.90	0.38	0.75	0.88
S5	17.48	5.13	3.75	8.53	65.11	0.42	1.00	1.04
S6	19.94	2.80	6.23	10.69	60.28	0.69	1.01	0.84
S7	17.86	1.95	6.93	9.75	63.51	0.78	0.96	0.91
S8	19.10	0.00	11.03	12.05	57.60	1.00	0.83	0.92

3.2. INVESTIGATION OF CONDUCTION MECHANISMS

The temperature dependences of the resistivity, $\rho(T)$, are presented in Fig. 1. It can be seen that all of the curves exhibit an activated character in the investigated samples (this will be seen better for plots of $\ln \rho/T$ vs. $1/T$). Also, the different

behavior of $\rho(T)$ curves with decreasing temperature is determined presumably by the different proximity to the metal-insulator transition (MIT), that has been often observed in kesterites [11,12,31–33].

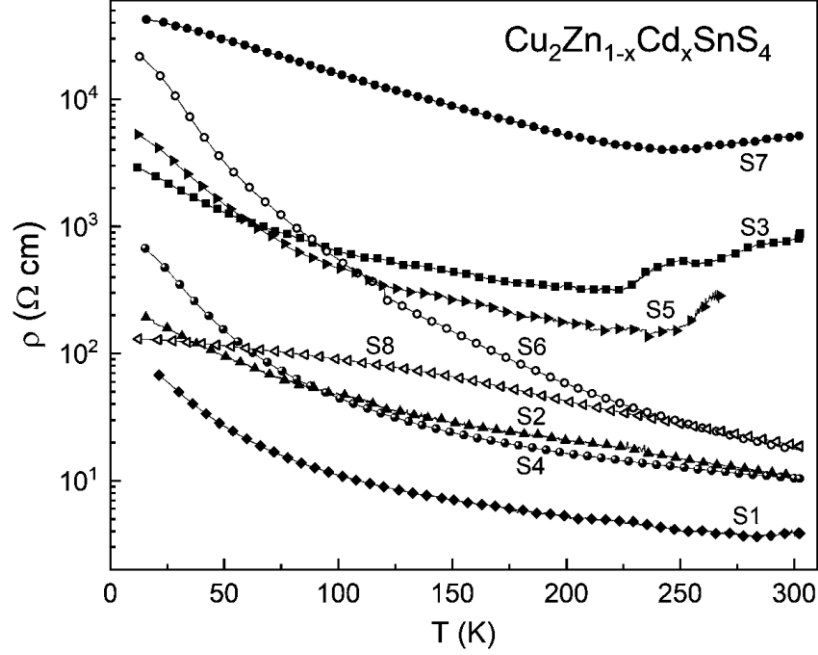


Fig. 1. Temperature dependence of the resistivity in the investigated CZCTS solid solutions.

The temperature dependence of the resistivity for the weakly doped crystalline semiconductors can be described by the following expression [34],

$$\rho(T) = A_p T^m \exp \left[\left(\frac{T_{0p}}{T} \right)^{1/p} \right], \quad (1)$$

suggesting different hopping regimes. Here, A_p is the prefactor constant, $p = 1$ refers to the nearest-neighbor hopping (NNH) conduction, $p = 4$ describes the Mott type of the variable-range hopping (VRH) conduction regime, T_{0p} represents the characteristic hopping temperature and $m = 1/p$.

The above mentioned equation describes the existence of several conduction mechanisms in quaternary compounds, as reported in literature [11–13]. For the kesterite compounds, the most expected of them are the NNH regime within a temperature interval ΔT_n , and the Mott VRH regime addressed to the interval ΔT_M . These mechanisms of conduction were observed in the large temperature intervals in our samples, too, and will be analyzed below. Our goal is to determine such

macroscopic parameters as ΔT_n , ΔT_M , the NNH activation energy E_n and the VRH characteristic temperature T_{04} . These data permits determination of the microscopic parameters a/a_0 , where a is the localization radius and a_0 is its value far from the MIT, the ratio of N/N_c (N is the acceptor concentration and N_c is its MIT value), as well as semi-width of the AB, W .

3.2.1. NNH conduction

We start the analysis of $\rho(T)$ using Eq. (1), for the case when $p = 1$, which corresponds to the NNH conduction. After the linearization of $\rho(T)$ curves with the plots of $\ln(\rho/T)$ vs. T^{-1} (Fig. 2), the data of ΔT_n and E_n are obtained and collected in Table 2. These values are in a good agreement with those reported in Ref. [35] for the CZCTS solid solutions within a smaller range of x .

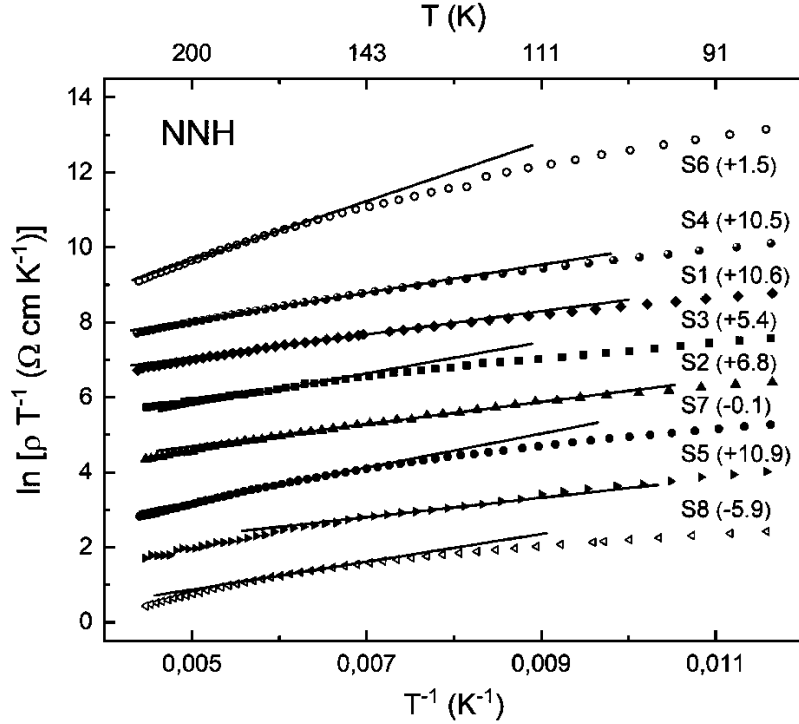


Fig. 2. The plots of $\ln(\rho/T)$ vs. T^{-1} for the investigated samples. For convenience the plots are shifted along the vertical axis by the values shown in parenthesis. The straight lines are linear fits.

3.2.2. Mott VRH conduction

The best linearization of the $\rho(T)$ curves was obtained for the case when $p = 4$, corresponding to the Mott VRH conduction. In this case the most linear temperature intervals were identified in the region of ~ 56 -142 K, which is in agreement with the intervals reported for the same family of compounds [11,31,36].

For this type of conduction, the characteristic temperature T_{04} is determined with the expression

$$T_{04} = \frac{\beta_4}{k_B g(\mu) a^3}, \quad (2)$$

where $\beta_4 \approx 21$ is a numerical constant, k_B is the Boltzmann constant, $g(\mu)$ represents the density of localized states (DOS) at the Fermi level, μ .

The a parameter is given by the following equation,

$$a = a_0 \left(1 - \frac{N}{N_c}\right)^{-\nu}, \quad (3)$$

Here $\nu \approx 1$ is a critical exponent of the correlation length [34,37,38].

The parameters a_0 and N_c are interrelated with the Mott criterion:

$$N_c^{1/3} a_0 \approx 0.25, \quad (4)$$

Using Eq. (2)-(4), and considering that $g(\mu) \approx N/(2W)$, where $W \approx 0.5k_B(T_v^3 T_{04})^{1/4}$ and T_v is the onset VRH temperature, the following equation can be obtained:

$$\left(\frac{T_{04}}{T_v}\right)^{1/4} \approx 4\beta_4^{1/3} \left(\frac{N_c}{N}\right)^{1/3} \left(1 - \frac{N}{N_c}\right)^\nu, \quad (5)$$

Numerical solution of Eq. (5) yields the values of the N/N_c . and then a/a_0 can be obtained with Eq. (3). These data are collected in Table 2.

Comparing the values of the ΔT_n interval with those of ΔT_M (Table 2), it can be clearly observed that they lie completely above ΔT_M , which satisfies the first requirement proposed in Ref. [35], for the observation of the NNH conduction.

The second requirement necessary for this purpose states that values of E_n and W parameters must be comparable, and it is satisfied for all samples excluding S8, as can be seen from Table 2. Such a big difference between values of E_n and W parameters may suggest that in this sample the charge transport is not provided by the pure NNH conduction, but more probably by a crossover between the Mott VRH and NNH conductions, or by other mechanism not connected to hopping [35].

Finally, the data above suggests, that the Fermi level μ lies close to the AB edge. In particular, this provides observation of both hopping regimes, as well as comparability of E_n and W .

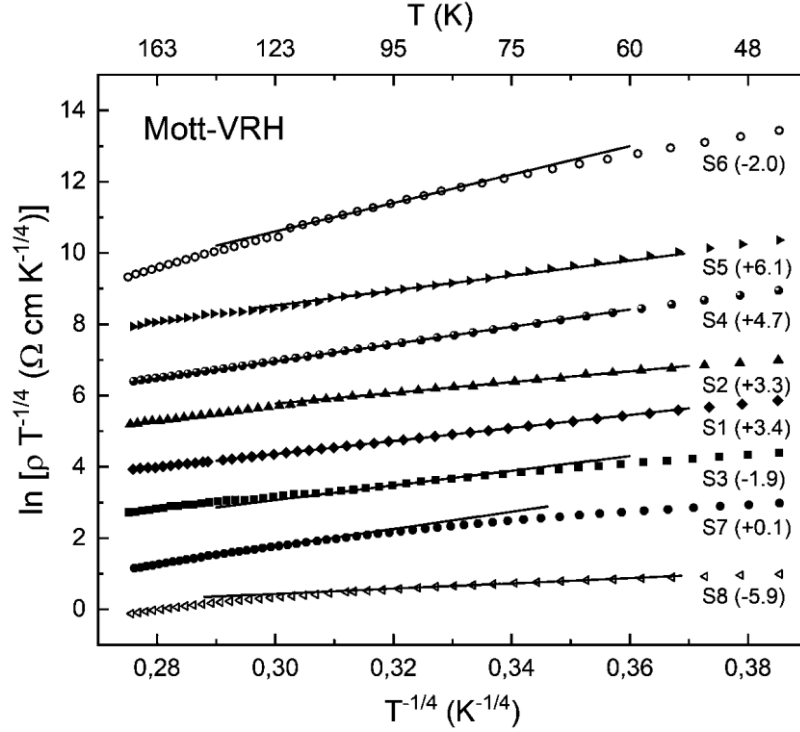


Fig. 3. The plots of $\ln(\rho/T^{1/4})$ vs. $T^{-1/4}$ for the investigated samples. For convenience the plots are shifted along the vertical axis by the values shown in parenthesis. The straight lines are linear fits.

Table 2.

Width of the NNH temperature interval (ΔT_n), the activation energy (E_n), width of the Mott VRH temperature interval (ΔT_M), the Mott VRH characteristic temperature (T_{04}), semi-width of the AB (W), the relative acceptor concentration (N/N_c) and localization radius in units of that far from the MIT (a/a_0).

Sample	ΔT_n (K)	E_n (meV)	ΔT_M (K)	T_{04} 10^3 (K)	W (meV)	N/N_c	a/a_0
S1	145-165	27	72-139	112.9	32	0.59	2.5
S2	109-151	25	56-95	52.08	20	0.63	2.7
S3	158-172	36	88-100	178.8	28	0.52	2.1
S4	150-167	32	100-135	342.2	41	0.49	2.0
S5	119-148	22	77-92	193.2	27	0.51	2.0
S6	170-192	68	84-110	2533	58	0.27	1.4
S7	159-175	39	123-142	341.7	43	0.50	2.0
S8	157-163	32	75-86	2.894	9	0.80	4.9

The obtained values of the temperature interval ΔT_M , for all investigated samples, are in good agreement with those reported in Ref. [11,35,39].

In the case of characteristic temperature T_{04} , the obtained values are of the same order with those reported in Ref. [35], excluding that of S6 for which it is significantly higher, than for the rest of the samples. This may be caused by the influence of a secondary phase in this sample.

In addition, for sample S8 (Table 2), all the obtained values of the parameters differ significantly from the other samples, addressed to the weaker temperature dependence of the resistivity, as shown in Fig. 3. This behavior can be determined by the closeness of this sample to the MIT, as reported in Ref. [33]. However, some influence of a secondary phase cannot be excluded in this case, too.

The dependences of W and E_n parameters on $\text{Cd}/(\text{Zn}+\text{Cd})$ ratio are shown in Fig. 4. From this figure it can be seen that these values show a non-monotonic behavior, exhibiting a maximum around ~ 0.69 value of the $\text{Cd}/(\text{Zn}+\text{Cd})$ ratio. The existence of this maximum can be related to the enhancement of the intrinsic disorder in the sample S6 due to the increased value of $W \sim 58$ meV, compared with that of $W \sim 11-25$ meV reported in CZTS single crystals [11,12].

Additionally, from Fig. 4 it can be observed that with increasing of Cd content in the samples, the value of W is decreased down to 9 meV, which can be related to the reduction of the Cu_{Zn} antisite defects in sample S8. This is because the formation of AB in most of the quaternary compounds is determined by the overwhelming effect of Cu_{Zn} antisite defects [14,40].

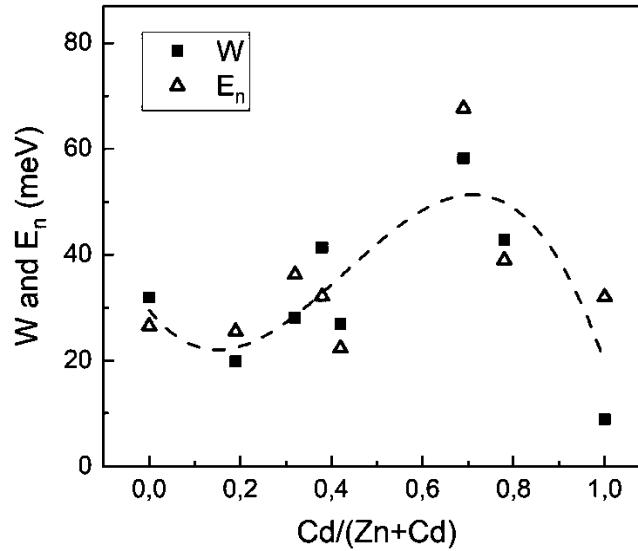


Fig. 4. The dependences of W and E_n on $\text{Cd}/(\text{Zn}+\text{Cd})$ ratio. The line is to guide the eye.

The obtained values of the N/N_c and a/a_0 are presented in Table 2 and correlates well with the data reported in Ref. [41]. Values of the N/N_c corresponding to the all of samples except the sample S6, are slightly high, being included within the interval $\sim 0.49-0.80$, whereas the corresponding values of the a/a_0 ratio, for the same samples, lie appreciably above unity. All of this suggests the proximity of this samples to the MIT [11].

On the other hand, for sample S6 the N/N_c ratio exhibit a value of 0.27, whereas the corresponding value of a/a_0 ratio is equal to 1.4, being closer to unity than for other samples. Therefore, the sample S6 lies relatively far from the MIT, such as the N/N_c ratio is enclosed in the interval $\sim 0.2-0.4$ [42], and value of a/a_0 ratio exceed unity only slightly, being included within the range $\sim 1.3-1.7$ [42].

Additionally, the sample S6 shows a minimum in the non-linear dependences of N/N_c and a/a_0 on the $\text{Cd}/(\text{Zn}+\text{Cd})$ ratio, displayed in Fig. 5. This minimum is correlated with the highest value of the $W \sim 58$ meV, which suggests a high level of intrinsic disorder in this sample.

The conjecture made above, regarding the sample S6, is also supported by the chemical composition, where for this sample the $(\text{Zn}+\text{Cd})/\text{Sn} = 0.84$. This deficit of Zn stimulates formation of the Zn vacancies, which can be occupied by Cu, forming the Cu_{Zn} antisite defects [43,44]. Therefore, the W exhibits a high value for sample S6 due to the Cu_{Zn} antisite defects, which act as acceptors.

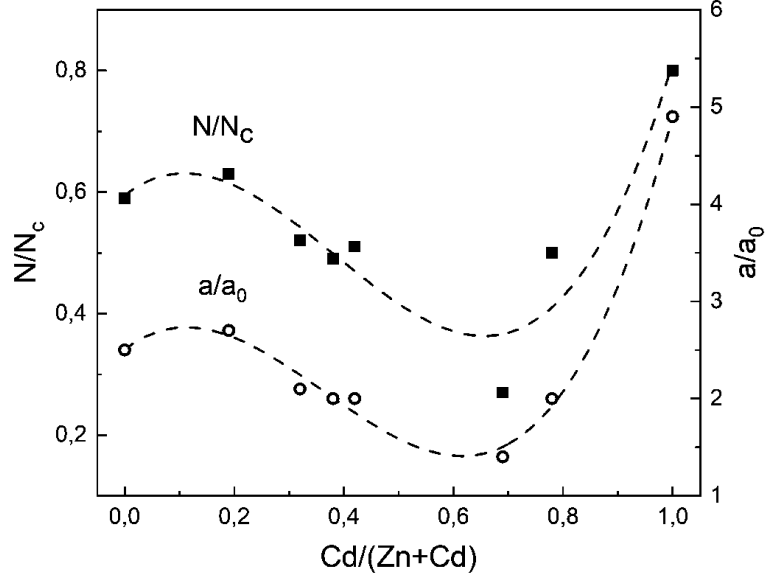


Fig. 5. The dependences of N/N_c and a/a_0 on $\text{Cd}/(\text{Zn}+\text{Cd})$ ratio. The lines are to guide the eye.

4. CONCLUSIONS

The resistivity of CZCTS solid solutions was investigated within the temperature range of 10-300 K. The linearization of $\rho(T)$ curves allowed to identify the presence of two conductivity mechanisms, the NNH conduction and the Mott VRH conduction mechanisms.

The NNH conduction was observed within the temperature interval of ~110-190 K, whereas the Mott VRH conduction was identified in the temperature range of ~55-140 K.

The NNH conduction was observed in all samples excluding S8, where the charge transport is most probably provided by a crossover between the Mott VRH and NNH conduction. For the rest of the samples, the presence of the NNH conduction is supported by the closeness of the values of activation energy E_n to the semi-width of the AB, W . This also indicates that the Fermi level μ lies close to the AB edge, in these samples.

Additionally, the parameters T_{04} , W , E_n , N/N_c and a/a_0 were obtained and the plots of W and E_n showed a non-monotonic behavior, exhibiting a maximum at around ~0.69 value of Cd/(Zn+Cd) ratio. The presence of this maximum can be related to the enhanced intrinsic disorder in the sample S6.

On the other hand, the curves of N/N_c and a/a_0 parameters also exhibited a non-linear behavior, showing a minimum near to ~0.69 value of the Cd/(Zn+Cd) ratio. As mentioned above, this minimum can be caused by the structural disorder in the investigated sample.

Finally, all the obtained results confirmed a relatively high level of intrinsic disorder in the case of sample S6, accompanied by a relatively far lying from the MIT. In contrast, for the rest of the samples, the analysis provided the evidence of proximity to the MIT.

Acknowledgements. This work was partially supported by the National Agency for Research and Development of the Republic of Moldova under the project 23.70105.5007.14T and the Ministry of Education and Research of the Republic of Moldova under the research sub-programme 011201.

The author is also very grateful to Senior Researcher I. A. Victorov for obtaining the monocrystalline samples by the chemical vapor transport method, and to L. Dermenji for measuring the elemental composition of the single crystal samples.

REFERENCES

1. A. Wang, M. He, M. A. Green, K. Sun, and X. Hao, *Advanced Energy Materials* **13**, 2203046 (2023).
2. S. Saha, *International Journal of Photoenergy* **2020**, **1** (2020).
3. M. He, C. Yan, J. Li, M. P. Suryawanshi, J. Kim, M. A. Green, and X. Hao, *Advanced Science* **8**, 2004313 (2021).
4. Q. Guo, G. M. Ford, W.-C. Yang, B. C. Walker, E. A. Stach, H. W. Hillhouse, and R. Agrawal, *J. Am. Chem. Soc.* **132**, 17384 (2010).
5. S. Bag, O. Gunawan, T. Gokmen, Y. Zhu, T. K. Todorov, and D. B. Mitzi, *Energy Environ. Sci.* **5**, 7060 (2012).
6. J. Zhou, X. Xu, B. Duan, H. Wu, J. Shi, Y. Luo, D. Li, and Q. Meng, *Nano Energy* **89**, 106405 (2021).
7. J. Fu, Q. Tian, Z. Zhou, D. Kou, Y. Meng, W. Zhou, and S. Wu, *Chem. Mater.* **28**, 5821 (2016).
8. O. Gunawan, T. K. Todorov, and D. B. Mitzi, *Applied Physics Letters* **97**, 233506 (2010).
9. I. L. Repins, H. Moutinho, S. G. Choi, A. Kanevce, D. Kuciauskas, P. Dippo, C. L. Beall, J. Carapella, C. DeHart, B. Huang, and S. H. Wei, *Journal of Applied Physics* **114**, 084507 (2013).
10. T. Gokmen, O. Gunawan, T. K. Todorov, and D. B. Mitzi, *Applied Physics Letters* **103**, 103506 (2013).
11. K. G. Lisunov, M. Guc, A. Nateprov, S. Levchenko, V. Tezlevan, and E. Arushanov, *Solar Energy Materials and Solar Cells* **112**, 127 (2013).
12. E. Lähderanta, M. Guc, M. A. Shakhov, E. Arushanov, and K. G. Lisunov, *Journal of Applied Physics* **120**, 035704 (2016).
13. E. Lähderanta, K. Lisunov, M. A. Shakhov, M. Guc, E. Hajdeu-Chicarosh, S. Levchenko, I. Zakharchuk, and E. Arushanov, *Journal of Magnetism and Magnetic Materials* **459**, 246 (2018).
14. S. Chen, A. Walsh, X. Gong, and S. Wei, *Advanced Materials* **25**, 1522 (2013).
15. S. Schorr, G. Gurieva, M. Guc, M. Dimitrievska, A. Pérez-Rodríguez, V. Izquierdo-Roca, C. S. Schnohr, J. Kim, W. Jo, and J. M. Merino, *J. Phys. Energy* **2**, 012002 (2020).
16. W. Wang, M. T. Winkler, O. Gunawan, T. Gokmen, T. K. Todorov, Y. Zhu, and D. B. Mitzi, *Advanced Energy Materials* **4**, 1301465 (2013).
17. L. H. Wong, A. Zakutayev, J. D. Major, X. Hao, A. Walsh, T. K. Todorov, and E. Saucedo, *J. Phys. Energy* **1**, 032001 (2019).
18. S. Kim, K. M. Kim, H. Tampo, H. Shibata, and S. Niki, *Appl. Phys. Express* **9**, 102301 (2016).
19. S. Giraldo, E. Saucedo, M. Nueschitzer, F. Oliva, M. Placidi, X. Alcobe, V. Izquierdo-Roca, S. Kim, H. Tampo, H. Shibata, A. Perez-Rodriguez, and P. Pisto, *Energy Environ. Sci.* (2017).
20. G. Sai Gautam, T. P. Senfile, and E. A. Carter, *Chem. Mater.* **30**, 4543 (2018).
21. C. Yan, K. Sun, J. Huang, S. Johnston, F. Liu, B. P. Veettil, K. Sun, A. Pu, F. Zhou, J. A. Stride, M. A. Green, and X. Hao, *ACS Energy Lett.* **2**, 930 (2017).
22. M. Pilvet, M. Kauk-Kuusik, M. Altosaar, M. Grossberg, M. Danilson, K. Timmo, A. Mere, and V. Mikli, *Thin Solid Films* **582**, 180 (2015).
23. Y. E. Romanyuk, S. G. Haass, S. Giraldo, M. Placidi, D. Tiwari, D. J. Fermin, X. Hao, H. Xin, T. Schnabel, M. Kauk-Kuusik, P. Pistor, S. Lie, and L. H. Wong, *J. Phys. Energy* **1**, 044004 (2019).
24. J. Li, D. Wang, X. Li, Y. Zeng, and Y. Zhang, *Advanced Science* **5**, 1700744 (2018).
25. K. C. Nwambaekwe, V. S. John-Denk, S. F. Douman, P. Mathumba, S. T. Yussuf, O. V. Uhuo, P. I. Ekwere, and E. I. Iwuoha, *Journal of Materials Research and Technology* **12**, 1252 (2021).
26. Z. Su, J. M. R. Tan, X. Li, X. Zeng, S. K. Batabyal, and L. H. Wong, *Advanced Energy Materials* **5**, 1500682 (2015).
27. S. R. Rondiya, Y. A. Jadhav, A. Živković, S. B. Jathar, G. K. Rahane, R. W. Cross, A. V. Rokade, R. S. Devan, S. Kolekar, R. L. Z. Hoye, H. N. Ghosh, N. H. De Leeuw, S. R. Jadhkar, and N. Y. Dzade, *Journal of Alloys and Compounds* **890**, 161575 (2022).
28. R. Sun, D. Zhuang, M. Zhao, Q. Gong, M. Scarpulla, Y. Wei, G. Ren, and Y. Wu, *Solar Energy Materials and Solar Cells* **174**, 494 (2018).

29. Z. Yuan, S. Chen, H. Xiang, X. Gong, A. Walsh, J. Park, I. Repins, and S. Wei, *Adv Funct Materials* **25**, 6733 (2015).
30. G. Gurieva, M. Guc, L. I. Bruk, V. Izquieredo-Roca, A. Perez-Rodriguez, S. Schorr, and E. Arushanov, *Physica Status Solidi C* **1** (2013).
31. K. G. Lisunov, M. Guc, S. Levchenko, D. Dumcenco, Y. S. Huang, G. Gurieva, S. Schorr, and E. Arushanov, *Journal of Alloys and Compounds* **580**, 481 (2013).
32. E. Lähderanta, E. Hajdeu-Chicarosh, M. A. Shakhov, M. Guc, I. V. Bodnar, E. Arushanov, and K. G. Lisunov, *J. Phys.: Condens. Matter* **28**, 455801 (2016).
33. M. Guc, R. Caballero, K. G. Lisunov, N. López, E. Arushanov, J. M. Merino, and M. León, *Journal of Alloys and Compounds* **596**, 140 (2014).
34. B. I. Shklovskii and A. L. Efros, "*Electronic Properties of Doped Semiconductors*", Springer-Verlag, Berlin-Heidelberg, 1984.
35. E. Lähderanta, E. Hajdeu-Chicarosh, V. Kravtsov, M. A. Shakhov, V. N. Stamov, I. V. Bodnar, E. Arushanov, and K. G. Lisunov, *New J. Phys.* **24**, 093008 (2022).
36. M. Guc, K. G. Lisunov, E. Hajdeu, S. Levchenko, V. Ursaki, and E. Arushanov, *Solar Energy Materials and Solar Cells* **127**, 87 (2014).
37. N. F. Mott and E. A. Davis, "*Electronic Processes in Non-Crystalline Materials*", 2nd ed. Clarendon press, Oxford, 2012.
38. N. F. Mott, "*Metal-Insulator Transitions*", Taylor & Francis, London, 1990.
39. E. Lähderanta, E. Hajdeu-Chicarosh, M. Guc, M. A. Shakhov, I. Zakharchuk, I. V. Bodnar, E. Arushanov, and K. G. Lisunov, *Sci Rep* **8**, 17507 (2018).
40. S. Chen, J.-H. Yang, X. G. Gong, A. Walsh, and S.-H. Wei, *Phys. Rev. B* **81**, 245204 (2010).
41. M. Guc, G. Gurieva, E. Hajdeu-Chicarosh, S. Schorr, K. G. Lisunov, and E. Arushanov, *Journal of Materials Research and Technology* **13**, 2251 (2021).
42. T. G. Castner, "*Hopping Conduction in the Critical Regime Approaching the Metal-Insulator Transition*", M. Pollak and B. Shklovskii (eds.), "*Hopping Transport in Solids*", North-Holland, Amsterdam, 1–47 (1991).
43. S. Chen, X. G. Gong, A. Walsh, and S.-H. Wei, *Applied Physics Letters* **96**, 021902 (2010).
44. A. Nagoya, R. Asahi, R. Wahl, and G. Kresse, *Phys. Rev. B* **81**, 113202 (2010).